Strong Ground Motion Attenuation Relationships for Subduction Zone Earthquakes

R.R. Youngs
S.-J. Chiou
Geomatrix Consultants

W.J. Silva
Pacific Engineering and Analysis

J.R. Humphrey
Lahontan GeoScience Inc.

ABSTRACT

We present attenuation relationships for peak ground acceleration and response spectral acceleration for subduction zone interface and intraslab earthquakes of moment magnitude M 5 and greater and for distances of 10 to 500 km. The relationships were developed by regression analysis using a random effects regression model that addresses criticism of earlier regression analyses of subduction zone earthquake motions. We find that the rate of attenuation of peak motions from subduction zone earthquakes is lower than that for shallow crustal earthquakes in active tectonic areas. This difference is significant primarily for very large earthquakes. The peak motions increase with earthquake depth and intraslab earthquakes produce peak motions that are about 50 percent larger than interface earthquakes.

INTRODUCTION

This paper presents attenuation relationships for subduction zone earthquakes. Two types of subduction zone earthquakes are considered, *interface* earthquakes and *intraslab* earthquakes. Subduction zone interface earthquakes are shallow angle thrust events that occur at the interface between the subducting and overriding plates. Examples include the 1964 M 9.2 Alaskan earthquake, and the 1985 M 8.0 Valpariso, Chile, and Michoacan, Mexico, earthquakes. Subduction zone intraslab earthquakes occur within the subducting oceanic plate and are typically high-angle, normal-faulting events responding to downdip tension in the subducting plate. Examples include the 1949 m_b 7.1 and 1965 M_S 6.5 earthquakes in the Puget Sound region of Washington State. In this paper, these two types of earthquakes are distinguished from *shallow crustal* earthquakes that occur in the upper 20 to 25 km of continental crust (such as the 1989 M 7.1 Loma Prieta, 1992 M 7.3 Landers, and 1994 M 6.7 Northridge earthquakes in California).

Published attenuation relationships for subduction zone earthquake motions (*e.g.*, Iwasaki *et al.*, 1978; Sadigh, 1979; Vyas *et al.*, 1984; Krinitzky *et al.*, 1987; Crouse *et al.*, 1988; Youngs *et al.*, 1988; Crouse, 1991) typically indicate that at distances greater than 50 km from the earthquake rupture, ground motions from these earthquakes are substantially larger than those from shallow crustal earthquakes in active tectonic regions. However, some investigators believe that the ground motions from interface earthquakes and shallow crustal earthquakes are similar, at least in Japan (Fukushima and Tanaka, 1990; Iai *et al.*, 1993). Both Fukushima and Tanaka (1990) and Iai *et al.* (1993) concluded that the reason previous researchers found lower attenuation rates for ground motions from Japanese earthquakes was that they employed a single stage regression analysis which was biased by correlations in the data. When Fukushima and Tanaka (1990) and Iai *et al.* (1993) used a two-staged regression technique similar to that employed by Joyner and Boore (1981), they found attenuation rates for shallow (depth less than 100 km) earthquake ground motions to be similar to that reported for crustal earthquakes in the western United States. Therefore, Fukushima and Tanaka (1990) and Iai *et al.* (1993) combined shallow crustal and subduction zone earthquake strong motions into a single data set to develop their attenuation relationships.

In this paper we restrict the data to subduction zone interface and intraslab strong motion recordings. To address the concerns raised by Fukushima and Tanaka (1990) and Iai (1993) we employ the random effects regression model of

Abrahamson and Youngs (1992), which is equivalent to a two-staged regression analysis (Brillinger and Preisler, 1985; Joyner and Boore, 1993). In addition, we use numerical simulations of large interface earthquakes to aid in judging the appropriateness of the attenuation models. The relationships given in this paper were first presented by Youngs *et al.* (1993).

STRONG MOTION DATA BASE

The data set analyzed in this study is summarized in Table 1. The magnitude measure used was Hanks and Kanamori's (1979) moment magnitude **M**. Source parameters of the earthquakes (epicenter location, focal depth, magnitude, and focal mechanism) were compiled from published special studies or the Harvard centroid moment tensor solutions. The Harvard solutions were used only for seismic moment M_o and focal mechanism. If no special study was found for an event, then earthquake location and magnitude given in the International Seismological Center or National Earthquake Information Center catalogs were used. If seismic moment was not reported, then the surface wave magnitude M_S was used, assuming that it is equivalent to moment magnitude in the magnitude range of 6 to 7.5 (Hanks and Kanamori, 1979). If only body wave magnitude m_b was reported, then m_b values in the range of 5 to 6 were converted to M_S using the relationship $M_S = 1.8m_b - 4.3$ proposed by Wyss and Habermann (1982) and the resulting value taken to be equivalent to moment magnitude. The differentiation between interface and intraslab events was done on the basis of the faulting mechanism, when reported, or on the basis of the focal depth, with events below a depth of 50 km considered to be intraslab events. Tichelaar and Ruff (1993) indicate that interface earthquakes worldwide nearly all occur at depths shallower than 50 km.

We characterized source-to-site distance in terms of the closest distance to the rupture surface, r_{rup}. If the rupture surface was not defined for an event, then hypocentral distance was used as the source-to-site distance. This is not expected to introduce a significant bias because rupture surfaces were defined for nearly all of the large events, and for the small events the difference between the minimum distance to rupture and hypocentral distance is small in comparison to the source-to-site distances for the recordings.

Based on published information on site conditions, the recordings were classified into three groups: rock, shallow stiff soil, and deep soil sites. Rock site conditions are expected to be similar to typical rock conditions in the California strong motion database, consisting of at most a few feet of soil over weathered rock. This classification is considered to be consistent with Boore *et al.* (1993) Site Class A near the boundary with Site Class B. Deep soil sites are those where the depth to bedrock is expected to be greater than 20 m. This site classification is considered to be consistent with Site Class C presented by Boore *et al.* (1993). The shallow stiff soil classification represents sites where the depth of soil is less than 20 m and a significant velocity contrast may exist within 30 m of the surface.

The data used in the analysis were restricted to free-field recordings from magnitude 5.0 and greater events. Free-field recordings are considered to be recordings obtained at the basement or the first floor levels of buildings less than four stories in height. In addition, data were excluded if the quality of the recorded acceleration time history was poor or if a portion of the main shaking was not recorded.

Figure 1 shows the magnitude-distance scattergram of the strong motion data set collected for analysis. The largest group of data is soil site data for interface events, primarily from Japan. A large portion of the rock data are from three Mexican subduction zone earthquakes recorded at the Guerrero Array. The 1992 M 7.0 Petrolia, California earthquake mainshock was also included as an interface event.

ANALYSIS OF PEAK HORIZONTAL ACCELERATIONS

Attenuation relationships for horizontal peak ground acceleration (PGA) from subduction zone earthquakes were evaluated by performing regression analyses on the empirical data. Because there are insufficient data to render stable estimates of the regression parameters individually for each of the six data groups, except for the interface soil data, we performed a joint regression analysis. The constants determined from the analyses include the attenuation relationship coefficients for the selected reference group and parameters representing the perturbations of the other five groups from the reference attenuation relationship. A set of indicator variables were used to identify data from each group: Z_t indicates source type (0 for interface events and 1 for intraslab events), Z_{di} indicates deep soil conditions (1 for deep soil sites and 0 otherwise), Z_{ss} indicates shallow stiff (1 for shallow soil sites and 0 otherwise), and Z_r indicates rock sites (1 for rock sites and 0 otherwise). The basic regression model follows the form used previously by Youngs *et al.* (1988) and Crouse (1991):

$$\ln(\mathrm{PGA})_{ij} = C_1^* + C_2\mathbf{M}_i + C_3^* \ln\left[(r_{rup})_{ij} + e^{C_4^* - \frac{C_2}{C_3^*}M_i}\right] + C_5 Z_t + C_9 H_i + C_{10} Z_{ss} + \eta_i + \varepsilon_{ij},$$

$$C_1^* = C_1 + C_6 Z_r \qquad (1)$$

$$C_3^* = C_3 + C_7 Z_r$$

$$C_4^* = C_4 + C_8 Z_r$$

where i is the earthquake index, j is the recording station index for the ith event, PGA (in units of g) is the geometrical mean of the two horizontal components of peak ground acceleration, **M** is moment magnitude, r_{rup} is the source-to-site distance (in kilometers), H is focal depth (in kilometers),

TABLE 1
List of Earthquakes Used to Develop Attenuation Relationships

Earthquake	Date	Lat.	Long.	*H* (km)	FT[1]	M	Distance Range	Number of Records[2]		
								RK	SS	DS
Alaska										
Alaska	1964.06.05	60.4	−146	16	t*	5.2	27.6–27.6	1	0	0
Alaska	1964.06.05	58.1	−152	13	t*	5	49.0–49.0	1	0	0
Alaska	1965.09.04	58.3	−153	32	t	6.8	68.3–68.3	1	0	0
Adak	1971.05.02	51.4	−177	38	t*	6.8	77.3–77.3	1	0	0
Shumagin Is	1974.04.06	54.9	−160	37	t	5.6	65.5–65.5	1	0	0
Shumagin Is	1974.04.06	54.9	−160	40	t	5.8	64.7–64.7	1	0	0
Alaska	1975.05.18	63.2	−150	106	n	5.4	144.1–144.1	0	0	1
St Elias	1979.02.28	60.6	−142	13	t	7.5	43.0–101.0	1	0	2
Alaska	1983.02.14	54.7	−159	25	t	6.5	40.4–126.0	2	1	0
Alaska	1983.02.14	54.9	−159	25	t	6	37.3–121.5	2	1	0
Alaska	1983.06.28	60.2	−141	19	t	5.9	23.1–23.1	1	0	0
	1985.10.09	54.7	−159	15	t	6.6	19.3–50.1	2	0	0
	1985.10.26	54.8	−159	18	t	5.3	20.5–20.5	1	0	0
	1985.11.14	54.7	−160	19	t	6	24.5–24.5	1	0	0
Andreanof Is	1986.05.07	51.5	−175	33	t	7.9	33.0–33.0	0	0	1
	1987.06.21	54.1	−162	33	t	6.5	47.0–47.0	1	0	0
Chile										
central Chile	1945.09.13	−34	−71	100	n*	7.1	107.7–107.7	0	1	0
central Chile	1952.04.29	−35	−72	10	t*	6	169.6–169.6	0	1	0
central Chile	1953.09.04	−33	−72	50	n*	6.4	144.8–144.8	0	1	0
central Chile	1958.09.04	−34	−70	15	t*	6.8	81.8–81.8	0	1	0
La Ligua	1965.03.28	−32	−71	72	n	7.4	145.7–145.7	0	1	0
central Chile	1967.09.26	−30	−72	48	n	5.6	396.0–396.0	0	1	0
Valparaiso	1971.07.09	−33	−71	42	t	7.8	101.0–101.0	0	1	0
central Chile	1973.10.05	−33	−72	23	t*	6.7	130.4–130.4	0	1	0
central Chile	1974.11.12	−33	−71	90	n*	6.2	94.0–96.7	1	1	0
central Chile	1978.12.21	−36	−72	46	t	5.8	66.3–127.7	0	0	3
central Chile	1979.07.05	−32	−71	52	n*	5.8	67.2–113.3	2	0	1
central Chile	1981.11.07	−32	−71	65	n	6.9	74.6–178.7	1	1	4
Valparaiso	1985.03.03	−33	−72	31	t	7.9	23.3–256.6	7	1	15
Valparaiso AS	1985.04.09	−34	−72	44	t	7.1	66.3–219.2	1	1	4
Cascadia										
Puget Sound	1949.04.13	47.2	−123	56	n	7.1	61.9–73.4	0	0	2
Seattle	1965.04.29	47.4	−122	63	n	6.7	88.9–88.9	0	0	1
Petrolia	1992.04.25	40.3	−124	11	t	7	8.5–71.1	2	4	8
Japan										
Chiba Pref	1956.02.14	35.7	140	45	n	6	46.6–46.6	0	1	0
Japan	1962.04.23	42.2	144	60	n	7	109.9–109.9	0	1	0
Ibaragi	1963.05.08	36.4	141	40	t*	6.1	65.5–65.5	0	1	0
Chiba	1963.08.04	35.4	140	39	t*	5.1	48.4–48.4	0	1	0
Ibaraki	1964.11.14	36.5	141	69	n	5.1	69.0–69.0	0	1	0

TABLE 1 (CONTINUED)
List of Earthquakes Used to Develop Attenuation Relationships

Earthquake	Date	Lat.	Long.	*H* (km)	FT[1]	M	Distance Range	Number of Records[2]		
								RK	SS	DS
Ibaragi	1967.11.19	36.4	141	48	t*	6	72.7–72.7	0	1	0
Hyuganada	1968.04.01	32.3	133	37	t	7.4	59.0–127.0	0	1	2
Hyuganada AS	1968.04.01	32.3	132	40	t	6.3	111.3–111.3	0	0	1
Tokachi-Oki	1968.05.16	40.7	144	20	t	8.2	102.9–550.9	0	5	10
Tokachi-Oki AS	1968.05.17	40.3	143	20	t	5.1	201.7–201.7	0	0	1
Iwate-Oki	1968.06.12	39.4	143	31	t	7.1	191.9–191.9	0	0	1
Saitama	1968.07.01	36	139	68	n*	6.1	84.8–84.8	0	0	1
W. Shikoku	1968.08.06	33.3	132	48	n	6.8	51.7–51.7	0	0	1
Hyuganada	1969.04.21	32.2	132	39	t	6.3	66.5–66.5	0	0	1
South Kurils	1969.08.00	43.6	147	30	t	8.2	240.9–240.9	0	1	0
Hokkaido	1970.01.20	42.4	143	25	t	6.4	43.9–124.9	0	1	1
Iwate	1970.04.01	39.8	142	75	n	5.8	76.4–126.1	0	1	1
Hyuganada	1970.07.25	32.1	132	47	t	7	55.0–71.7	0	1	1
Hyuganada As	1970.07.26	32.1	132	47	t	5.9	72.2–72.2	0	0	1
Aichi	1971.01.04	34.4	137	44	n	6.1	87.4–87.4	0	0	1
Erimomisaki	1971.08.02	41.2	144	45	n	7.1	159.0–263.5	0	1	1
Chiba	1971.10.11	35.9	141	40	t	5.2	42.4–42.4	0	1	0
Hachijojima	1972.02.29	33.2	141	50	t	7.4	295.1–307.6	0	1	2
	1972.03.19	40.9	142	80	n	6.4	97.2–203.2	0	0	2
Kushiro, j044	1972.05.11	42.6	145	63	n*	5.8	88.4–88.4	0	1	0
Bonin	1972.12.04	33.2	141	50	t	7.5	286.1–417.9	0	0	2
Nemuro-Oki	1973.06.17	43	146	41	t	7.8	99.0–99.0	0	1	0
Chiba	1974.03.03	35.6	141	49	t	5.6	65.6–65.6	0	1	0
Ibaragi	1974.07.08	36.4	141	45	t	6	83.6–83.6	0	1	0
Tomskomai	1974.11.08	42.5	142	125	n*	6.5	126.8–251.0	0	1	1
Chiba	1974.11.15	35.8	141	44	t	5.6	69.4–69.4	0	1	0
	1978.02.20	38.8	142	50	t	6.5	121.9–537.0	0	2	10
South Kurils	1978.03.24	44.2	149	31	t	7.5	389.3–389.3	0	1	0
Miyagi-Ken-Oki	1978.06.12	38.2	142	40	t	7.6	93.0–475.1	0	4	13
	1979.07.11	36.6	141	40	t	5.9	65.3–196.7	0	1	3
	1979.07.13	33.9	132	70	n	6.1	162.0–162.0	0	0	1
	1980.09.23	36	140	80	n	5.3	89.1–114.1	0	1	3
	1981.01.23	42.4	142	130	n	6.8	161.0–744.2	0	1	6
	1981.12.02	40.9	143	60	n	6.3	118.0–220.7	0	0	5
	1982.03.21	42.1	143	40	t	6.9	75.5–207.7	0	1	5
	1982.03.21	42.2	143	18	t	5.5	71.3–129.8	0	0	2
E off Kanto	1982.07.23	36.2	142	30	t	7	119.9–356.9	0	1	5
Nihonkai-Chubu	1983.05.26	40.4	139	14	t	7.7	81.7–166.6	0	1	5
W off N Tohoku	1983.06.09	40.2	139	23	t	5.9	121.2–233.7	0	1	2
	1983.06.09	40.2	139	14	t	5.9	121.5–166.7	0	1	1
W off N Tohoku	1983.06.21	41.3	139	20	t	6.8	157.4–272.6	0	1	4
	1984.01.17	36.5	141	43	t	5.5	87.2–186.1	0	1	1

TABLE 1 (CONTINUED)
List of Earthquakes Used to Develop Attenuation Relationships

Earthquake	Date	Lat.	Long.	*H* (km)	FT[1]	M	Distance Range	Number of Records[2]		
								RK	SS	DS
	1984.01.17	36.5	141	43	t	5.7	88.2–187.5	0	1	1
	1984.03.06	42.5	143	118	n	5.7	125.2–202.6	0	0	2
SE off Kyushu	1984.08.06	32.4	132	33	n	6.9	93.0–184.1	0	0	2
	1984.09.18	34.1	142	13	n	6.8	223.5–232.7	0	1	1
	1985.03.28	40.3	141	164	n	6.3	178.6–357.8	0	1	3
	1985.05.13	33	133	39	n	5.5	114.2–167.4	0	0	2
	1986.02.12	36.4	141	44	t	6.2	73.5–160.4	0	1	2
	1986.11.28	36.4	141	42	t	5.8	78.8–177.1	0	1	3
	1987.01.14	42.5	143	119	n	6.8	126.2–513.4	0	1	6
	1987.02.06	36.9	142	30	t	6.4	160.0–174.6	0	1	1
E off Fukushima Pr	1987.02.06	37	142	35	t	6.7	94.4–402.3	0	1	7
	1987.03.18	32	132	48	n	6.6	76.7–226.1	0	0	2
	1987.04.07	37.3	142	44	t	6.6	103.9–288.7	0	1	6
	1987.04.16	37	142	45	t	6	157.0–159.6	0	0	2
	1987.04.22	37.1	142	47	t	6.6	80.9–260.1	0	1	5
	1987.05.11	38.9	142	50	t	5.8	123.1–206.6	0	0	4
	1987.09.24	36.6	141	41	t	5.9	64.1–202.7	0	1	5
Mexico										
Mexico	1962.05.11	17.3	–100	40	t	7.2	248.6–248.6	0	0	1
Mexico	1962.05.19	17.1	–100	33	t	7.2	262.3–262.3	0	0	1
Mexico	1962.11.30	17.3	–99	57	n*	5.8	245.1–245.1	0	0	1
Mexico	1964.07.06	18	–101	100	n	7.4	242.0–252.9	1	0	3
Mexico	1965.08.23	16.3	–96	16	t	7.4	473.4–481.3	1	0	1
Mexico	1965.12.09	17.3	–100	57	n*	6.3	77.0–261.0	1	0	1
Mexico	1966.04.11	18	–103	30	t*	5.5	100.0–100.0	1	0	0
Mexico	1966.09.25	18.3	–101	79	n	5.7	140.7–140.7	1	0	0
Mexico	1968.07.02	17.6	–100	41	n	6.5	104.8–236.6	1	0	1
Mexico	1968.08.02	16.6	–98	16	t	7.3	192.6–330.0	2	0	1
Mexico	1971.09.05	17.1	–100	50	n*	5	56.7–56.7	0	0	1
Mexico	1973.08.28	18.3	–97	84	n	7.1	156.1–296.6	0	0	4
Mexico	1975.03.14	16.6	–93	155	n	5.6	158.5–158.5	0	0	1
Mexico	1976.06.07	17.4	–101	45	t*	6.4	109.2–109.2	0	0	1
Mexico	1978.03.19	17	–100	36	t	6.6	43.9–43.9	0	0	1
Oaxaca	1978.11.29	16	–97	18	t	7.7	122.3–424.2	1	1	4
Oaxaca 1st AS	1978.11.29	16.2	–97	33	t	5.2	107.5–437.2	1	1	1
Oaxaca 2nd AS	1978.11.29	16.2	–97	22	t	6	102.3–441.7	1	1	1
Guerrero	1979.03.14	17.5	–101	20	t	7.4	71.4–351.1	2	1	11
Mexico	1981.09.17	16.8	–99	22	t*	5.4	22.3–54.6	0	0	2
Playa Azul	1981.10.25	17.8	–102	20	t	7.2	23.6–422.2	3	1	13
Michoacan	1985.09.19	18.2	–103	18	t	8	12.9–358.7	16	3	9
Michoacan AS	1985.09.21	18	–101	15	t	7.5	24.4–191.6	11	1	1
Michoacan AS	1985.10.29	17.6	–103	20	t	5.9	59.1–59.1	1	0	0

TABLE 1 (CONTINUED)
List of Earthquakes Used to Develop Attenuation Relationships

Earthquake	Date	Lat.	Long.	*H* (km)	FT[1]	M	Distance Range	Number of Records[2]		
								RK	SS	DS
Michoacan	1986.04.30	18	–103	20	t	6.9	38.2–90.6	2	0	0
Michoacan AS	1986.05.05	17.8	–103	20	t	5.9	39.6–39.6	1	0	0
Guerrero	1986.05.29	16.9	–99	36	t	5.2	49.3–95.1	5	0	0
	1989.04.25	16.6	–99	19	t	6.9	18.4–197.4	14	0	2
Peru										
Peru	1947.11.01	–11	–75	30	t*	7.7	271.0–271.0	0	1	0
Peru	1951.01.31	0	0	50	n*	6	116.0–116.0	0	1	0
Peru	1952.08.03	0	0	50	n*	5.3	125.0–125.0	0	1	0
Peru	1957.01.24	0	0	50	n*	6.3	120.0–120.0	0	1	0
Peru	1957.02.18	0	0	100	n	6.5	152.0–152.0	0	1	0
Peru	1966.10.17	–11	–79	24	t	8.1	164.9–164.9	0	1	0
Peru	1970.05.31	–9.4	–79	56	n	7.9	259.4–259.4	0	1	0
Peru	1971.11.29	–11	–78	54	n	5.3	131.7–131.7	0	1	0
Peru	1974.01.05	–12	–76	98	n	6.6	131.1–131.3	0	2	0
Peru	1974.10.03	–12	–78	27	t	8.1	70.8–73.8	0	2	0
Peru, AS	1974.11.09	–12	–77	30	t	7	68.3–74.6	0	1	1
Solomon Islands										
Long Island	1967.11.14	–5.5	147	194	n*	5.8	243.4–243.4	0	0	1
Long Is	1968.04.29	–5.4	146	31	t*	5.8	101.1–101.1	0	0	1
Long Is	1968.06.03	–5.5	147	182	n*	5.6	226.5–226.5	0	0	1
N. Huon	1968.06.17	–6.3	147	106	n*	5.2	124.0–124.0	0	0	1
New Britain	1968.09.16	–6.1	149	49	n*	6.3	313.5–313.5	0	0	1
Arona	1969.01.07	–6.2	146	111	n*	5.1	122.3–122.3	0	0	1
Umboi Is	1968.03.10	–5.6	147	194	n*	6	232.1–252.6	0	0	2
Umboi Is	1969.06.24	–5.9	147	117	n*	5.2	152.6–153.9	0	0	2
Lae	1969.08.02	–6.5	147	33	t*	5.1	40.1–40.1	0	0	1
Danfu	1969.08.03	–4.3	153	59	n*	5.4	112.9–112.9	0	0	1
Taki	1969.09.07	–6.6	156	174	n*	5.1	179.1–179.1	0	1	0
Ulingan	1970.10.31	–4.9	145	42	t	7	162.0–162.0	0	0	1
Wasu	1971.02.12	–6.3	147	123	n*	5.8	135.9–142.7	0	0	2
Wasu	1971.02.13	–6.1	146	114	n*	5.4	119.7–157.9	0	0	2
Madang	1971.03.13	–5.8	145	114	n*	6.9	142.2–142.2	0	0	1
New Britain Is	1971.07.14	–5.5	154	43	t	8	153.0–153.0	0	1	0
Annanberg	1971.07.19	–4.9	145	75	n*	5.8	232.1–232.1	0	0	1
New Ireland Is	1971.07.26	–4.9	153	43	t	8.1	251.0–251.0	0	1	0
New Britain Is	1971.09.14	–6.5	152	22	t*	6.3	258.7–258.7	0	0	1
Lae	1971.09.25	–6.5	147	111	n*	7	119.1–119.1	0	0	1
Kokopo	1971.10.14	–4.4	152	25	t*	5.6	38.3–38.3	0	0	1
Buka Is	1971.10.28	–5.6	154	107	n*	6.5	271.1–271.1	0	0	1
Long Is	1972.11.05	–5.4	147	229	n*	5.4	273.5–273.5	0	0	1
Marienberg	1973.08.13	–4.5	144	109	n*	6.3	304.1–418.6	0	0	2
Saidor	1974.03.25	–6	146	110	n*	5.4	113.1–113.1	0	0	1

TABLE 1 (CONTINUED)
List of Earthquakes Used to Develop Attenuation Relationships

Earthquake	Date	Lat.	Long.	*H* (km)	FT[1]	M	Distance Range	Number of Records[2]		
								RK	SS	DS
Saidor	1974.09.20	–6.2	146	105	n*	6.1	106.0–106.1	1	0	1
Solomon Is	1981.12.13	–6.4	155	50	t	5.8	79.6–79.6	1	0	0
Solomon Is	1981.12.13	–6.3	155	48	t	5.4	78.6–78.6	1	0	0

1. t = interface thrust, n = intraslab, * indicates mechanisms inferred by depth
2. RK = rock, SS = shallow soil, DS = deep soil

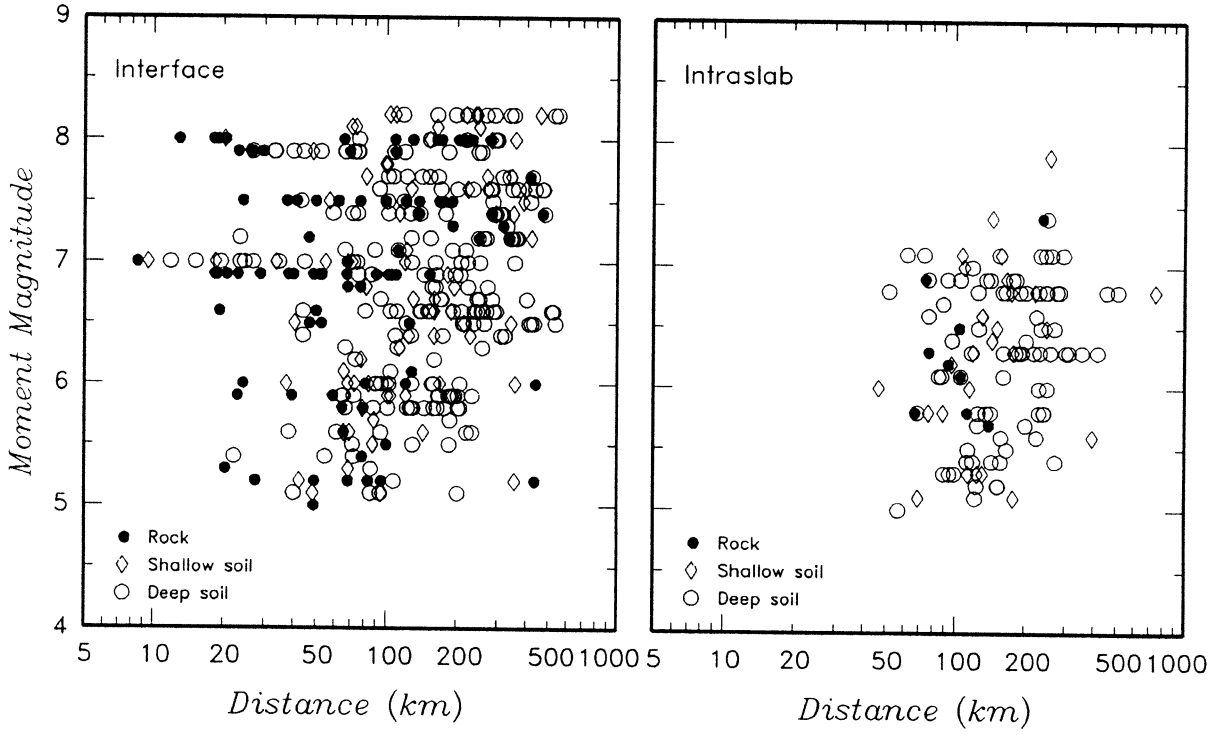

▲ **Figure 1.** Scattergram of subduction zone PGA data set.

and C_k, k = 1 to 10, are coefficients determined by regression analysis. The terms H and Z_{ss} are additions to the Youngs *et al.* (1988) model. Crouse *et al.* (1988) first proposed that peak motions are proportional to the depth of the event. In contrast, Youngs *et al.* (1988) found that the depth effect observed by Crouse *et al.* (1988) could be explained by accounting for a difference between interface and intraslab events. In this analysis we find that both effects are significant. Recently, Molas and Yamazaki (1995) also report that there is a significant correlation between depth and peak amplitude for Japanese subduction zone strong motion data. The error term in (1) is partitioned into an inter-event component η_i representing the earthquake-to-earthquake variability of ground motions, and an intra-event component ε_{ij} representing within earthquake variability of ground motions. The terms η_i and ε_{ij} are assumed to be independent normally distributed variates with variances τ^2 and σ^2, respectively. Following the model developed by Youngs *et al.* (1995), variance terms τ and σ were assumed to be linear functions of magnitude. The regression coefficients and the error terms η_i and ε_{ij} were obtained by the random effects regression algorithm described in Abrahamson and Youngs (1992). Figure 2 compares the fitted relationships to PGA data from interface earthquakes recorded on rock and deep soil sites.

The recorded strong motion data shown on Figure 2 display a large difference between rock and soil site PGAs at all distances. The attenuation relationships fit to the data predict that the ratio of soil to rock PGA increases as the ground motion level increases. This result is contrary to what

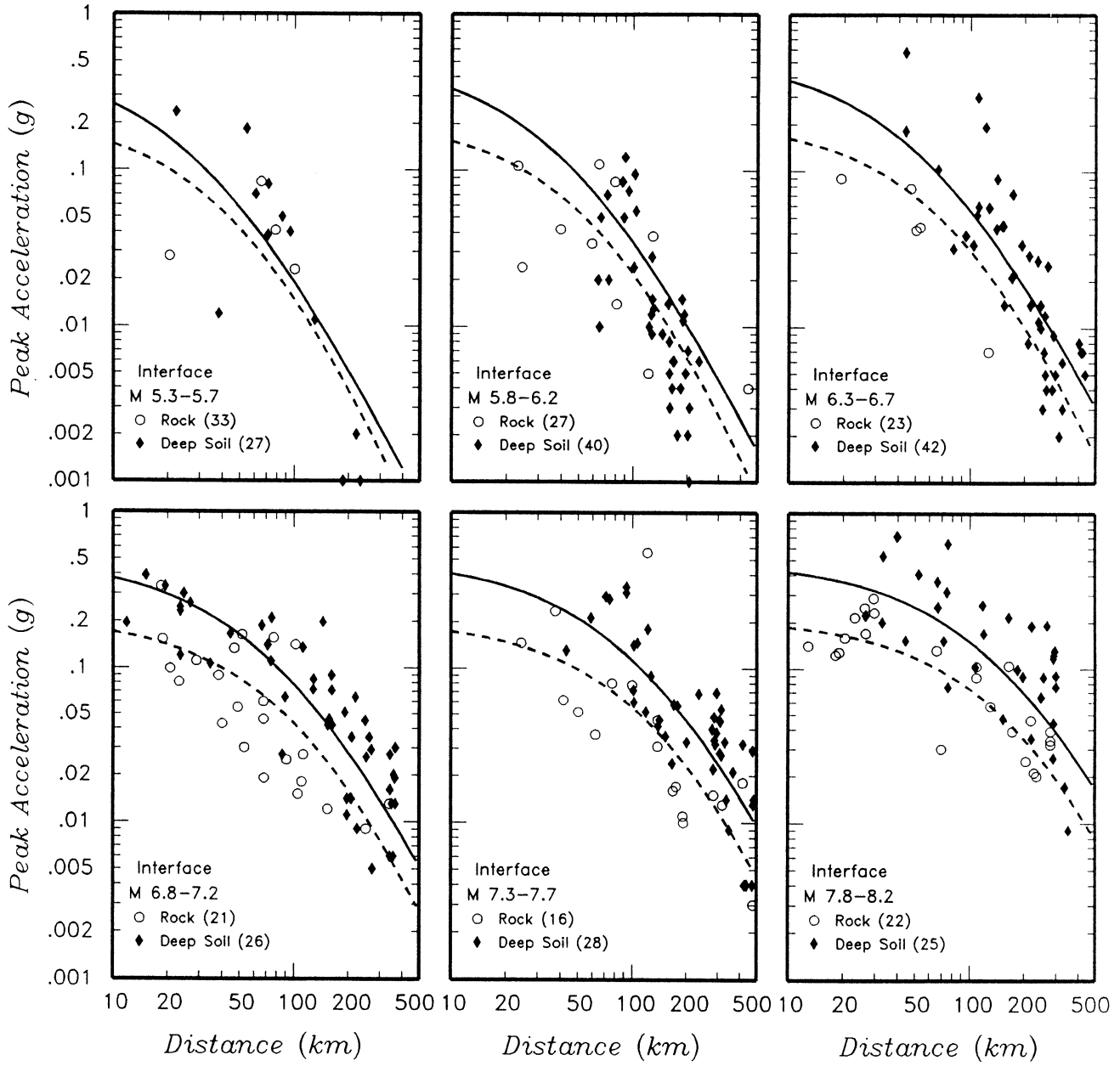

▲ **Figure 2.** Comparison of PGA values predicted using regression model (1) and the empirical data for interface earthquakes. Numbers in parentheses give the average depth of earthquakes in each data subset. The solid line is the attenuation relationship fit to deep soil site data and the dashed line is the relationship fit to the rock site data.

one would expect because nonlinear soil effects should reduce soil amplification as the level of shaking increases. We examined the expected difference between soil and rock PGA by performing numerical simulations of ground motions on rock and soil sites from a **M** 8 subduction zone earthquake using the finite-source form of the stochastic ground motion model (Silva and Stark, 1992). The simulations incorporated site effects through a one-dimensional wave propagation model coupled with the equivalent-linear representation of soil properties (Silva, 1991). Humphrey *et al.* (1993) were able to produce a good fit to strong motions from the 1985 Valpariso and Michoacan earthquakes using this simulation model.

Figure 3 compares the results of the simulations for rock, shallow soil (20 ft depth) and deep soil (120 ft and 500 ft depths) to the results of the regression analysis using (1). There is good agreement between the simulations and the empirical model at distances greater than 50 km. At smaller distances, the simulations indicate convergence of the rock and deep soil site peak motions with decreasing distance. In the near field, the simulations produced higher motions than those predicted by the empirical model (1).

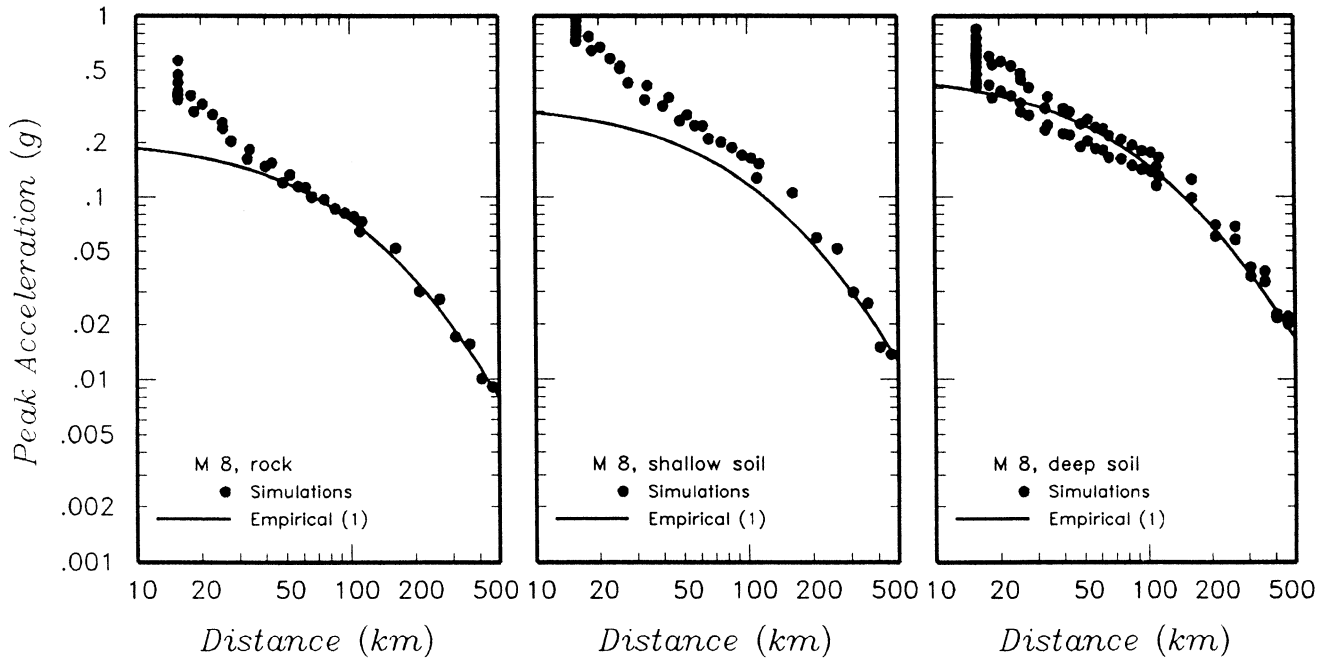

▲ **Figure 3.** Comparison of PGA values predicted using regression model (1) and finite-fault stochastic model simulations.

The fitted empirical relationships are poorly constrained at small distances due to lack of data from multiple earthquakes. Therefore, the form of the regression model was modified to force convergence of the predictions for soil and rock motions at very small distances. The modified model is given by:

$$\ln(\mathrm{PGA})_{ij} = C_1^* + C_2\mathbf{M}_i + C_3^* \ln\left[(r_{rup})_{ij} + e^{C_4^* - \frac{C_2}{C_3^*}\mathbf{M}_i}\right] + C_5 Z_{ss} + C_8 Z_t + C_9 H_i + \eta_i + \varepsilon_{ij},$$

$$C_1^* = C_1 + C_3 C_4 - C_3^* C_4^* \qquad (2)$$

$$C_3^* = C_3 + C_6 Z_s$$

$$C_4^* = C_4 + C_7 Z_s$$

When (2) was fit to the data, the resulting relationships predicted higher PGA values for rock in the near field than obtained using (1), but lower soil PGA values. The reduction in near field soil amplitudes is likely due to the lack of near field soil data. Therefore, we judged it appropriate to use the soil attenuation model obtained by fitting model (1) and the rock attenuation model obtained by fitting model (2). The selected attenuation models are listed in Table 2. Figure 4 compares the selected attenuation relationships to the recorded PGA data.

The issue of near field motions was further examined by conducting simulations of rock site motions for **M** 7, 8, and 8.5 interface events. Figure 5 compares the results of these simulations to the PGA values predicted by the relationship for interface earthquakes listed in Table 2. At distances greater than 30 to 40 km, the simulations compare well with the empirical interface model. At smaller distances, the simulations predict higher motions than the empirical interface model for all three magnitudes. Also shown on Figure 5 are PGA values predicted by a shallow crustal attenuation relationship for rock motions from reverse faulting earthquakes (Sadigh *et al.*, 1993). The near field simulations results are consistent with the shallow crustal attenuation model.

Figure 6 compares the PGA predictions from the attenuation models listed in Table 2 to those obtained by Crouse (1991), Fukushima and Tanaka (1990), and Iai *et al.* (1993) for **M** 6, 7, and 8 interface earthquakes. The Crouse (1991) soil model predicts PGA values that are very similar to those obtained using the deep soil model listed in Table 2. The Fukushima and Tanaka (1990) model predictions are consistent with the model developed in this study for **M** 6 events but tend to give much lower results at large distances as the magnitude of the earthquake increases. These comparisons suggest that the differences between PGA attenuation of shallow crustal and interface earthquakes are significant primarily for very large earthquakes. Unlike the other three attenuation relationships shown on Figure 6, the model proposed by Iai *et al.* (1993) does not include the effect of near field magnitude saturation. Thus, while it predicts motions consistent with the other models at magnitudes and distances within the bulk of the data, it does not match the other models at small distances, underpredicting the other models at **M** 6 and greatly overpredicting the other models at **M** 8.

The results of the regression analyses of the PGA data indicated that intraslab earthquakes produce peak motions

TABLE 2
Attenuation Relationships for Horizontal Response Spectral Acceleration (5% Damping) for Subduction Earthquakes

For Rock

$$\ln(y) = 0.2418 + 1.414\mathbf{M} + C_1 + C_2(10-\mathbf{M})^3 + C_3 \ln\left(r_{rup} + 1.7818e^{0.554\mathbf{M}}\right) + 0.00607H + 0.3846Z_T$$

Standard Deviation $= C_4 + C_5\mathbf{M}$

Period(s)	C_1	C_2	C_3	C_4*	C_5*
PGA	0.0	0.0	−2.552	1.45	−0.1
0.075	1.275	0.0	−2.707	1.45	−0.1
0.1	1.188	−0.0011	−2.655	1.45	−0.1
0.2	0.722	−0.0027	−2.528	1.45	−0.1
0.3	0.246	−0.0036	−2.454	1.45	−0.1
0.4	−0.115	−0.0043	−2.401	1.45	−0.1
0.5	−0.400	−0.0048	−2.360	1.45	−0.1
0.75	−1.149	−0.0057	−2.286	1.45	−0.1
1.0	−1.736	−0.0064	−2.234	1.45	−0.1
1.5	−2.634	−0.0073	−2.160	1.50	−0.1
2.0	−3.328	−0.0080	−2.107	1.55	−0.1
3.0	−4.511	−0.0089	−2.033	1.65	−0.1

For Soil

$$\ln(y) = -0.6687 + 1.438\mathbf{M} + C_1 + C_2(10-\mathbf{M})^3 + C_3 \ln\left(R + 1.097e^{0.617\mathbf{M}}\right) + 0.00648H + 0.3643Z_T$$

Standard Deviation $= C_4 + C_5\mathbf{M}$

Period(s)	C_1	C_2	C_3	C_4*	C_5*
PGA	0.0	0.0	−2.329	1.45	−0.1
0.075	2.400	−0.0019	−2.697	1.45	−0.1
0.1	2.516	−0.0019	−2.697	1.45	−0.1
0.2	1.549	−0.0019	−2.464	1.45	−0.1
0.3	0.793	−0.0020	−2.327	1.45	−0.1
0.4	0.144	−0.0020	−2.230	1.45	−0.1
0.5	−0.438	−0.0035	−2.140	1.45	−0.1
0.75	−1.704	−0.0048	−1.952	1.45	−0.1
1.0	−2.870	−0.0066	−1.785	1.45	−0.1
1.5	−5.101	−0.0114	−1.470	1.50	−0.1
2.0	−6.433	−0.0164	−1.290	1.55	−0.1
3.0	−6.672	−0.0221	−1.347	1.65	−0.1
4.0	−7.618	−0.0235	−1.272	1.65	−0.1

y = spectral acceleration in g
M = moment magnitude
r_{rup} = closest distance to rupture (km)
H = depth (km)
Z_T = source type, 0 for interface, 1 for intraslab
* Standard deviation for magnitudes greater than **M** 8 set equal to the value for **M** 8

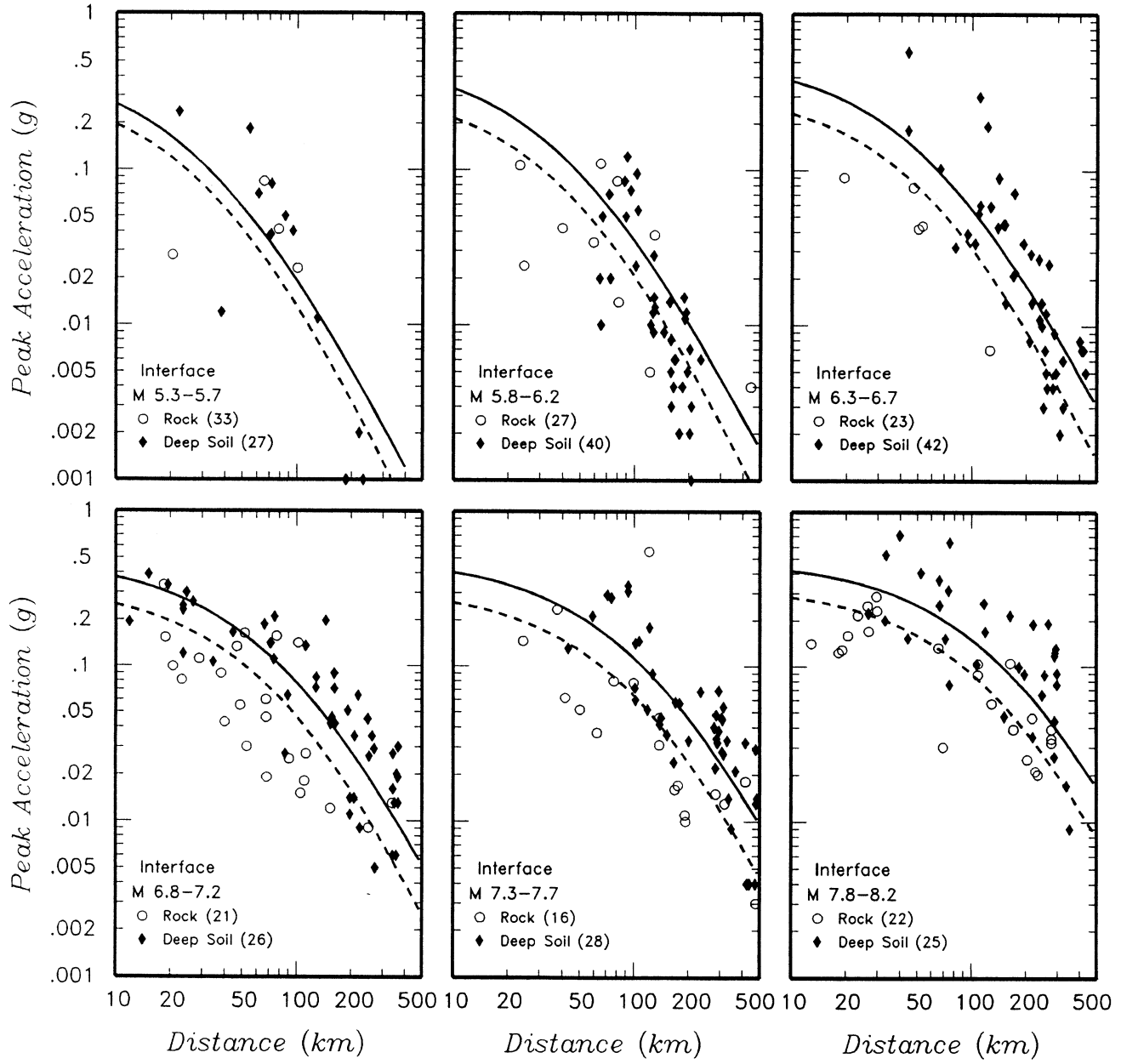

▲ **Figure 4.** Comparison of PGA values predicted using attenuation models listed in Table 2 and the empirical data for interface earthquakes. Numbers in parentheses give the average depth of earthquakes in each data subset. The solid line is the attenuation relationship fit to deep soil site data and the dashed line is the relationship fit to the rock site data.

that are on average about 50 percent higher than those for interface earthquakes for the same magnitude and distance. Figure 7 compares the predicted PGA values for intraslab earthquakes with the recorded data.

ANALYSIS OF RESPONSE SPECTRA ORDINATES

The number of digitized and processed accelerograms for subduction zone earthquakes is only a subset of the PGA database and is often limited to recordings with the strongest shaking from each earthquake. Therefore, attenuation relationships for peak response spectral acceleration (SA) fitted directly to the calculated peak spectral ordinates may be biased. We therefore developed relationships for response spectral amplification (SA/PGA). We followed the approach of Youngs *et al.* (1988) and included both magnitude and distance effects on response spectral amplification. The spectral amplification relationship for any one spectral period is

$$\ln\left(\mathrm{SA/PGA}\right)_{ij} = B_1 + B_2\left(10-\mathbf{M}_i\right)^3 + B_3 \ln\left[\left(r_{rup}\right)_{ij} + e^{\alpha_1+\alpha_2\mathbf{M}_i}\right] \quad (3)$$

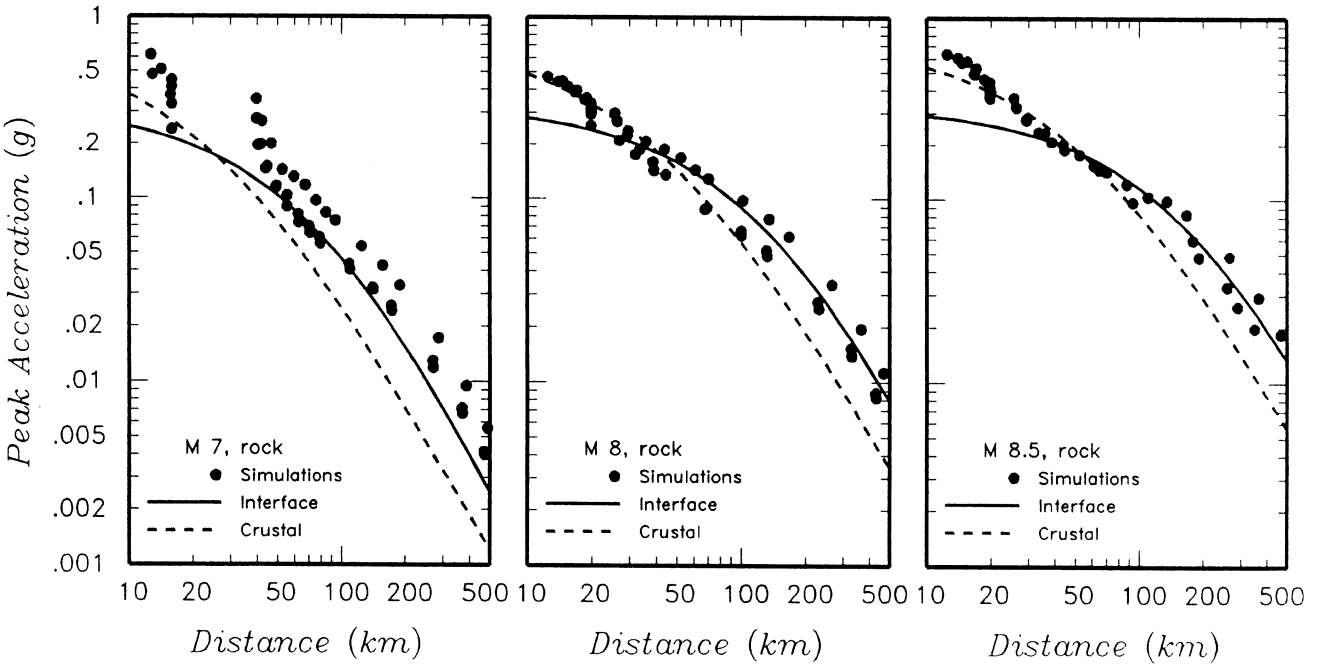

▲ **Figure 5.** Comparison of PGA values predicted using the interface relationship for rock sites listed in Table 2 and finite-fault stochastic model simulations for **M** 7, 8, and 8.5 events. Also shown are PGA values predicted using the shallow crustal model of Sadigh *et al.* (1993).

The second term accounts for the magnitude scaling of ground motions, and the third term for distance dependence. The coefficients α_1 and α_2 are set equal to the coefficients C_4 and C_5 of the appropriate PGA attenuation relationship. The remaining variables have the same meaning as those used in the PGA regression model. The coefficients obtained at individual periods were then smoothed so that the resulting spectral shapes are smooth over the full range of magnitudes and distances. Coefficients B_2 and B_3 were found to be nearly linearly dependent on the log of spectral period. Figure 8 shows the resulting spectral shapes for **M** 6.5, 7.5, and 8.5 events at distances of 50 and 200 km. The soil and rock spectral shapes are similar for smaller magnitudes and then begin to diverge at larger magnitudes, with the soil spectral shape having more long-period motion, as one would expect. The spectral shapes developed in this study for soil site motions are similar to those derived from the analysis presented by Crouse (1991).

The coefficients obtained by fitting (3) to spectral amplification values were then combined with the appropriate attenuation relationships for PGA to produce attenuation relationships for 5% damped SA. These relationships are listed in Table 2.

GROUND MOTION VARIABILITY

The remaining component of the attenuation relationships is an assessment of the variability of the peak motions of individual recordings about the median attenuation relationships listed in Table 2. We followed the standard convention and assumed that the individual peak motions are lognormally distributed. Youngs *et al.* (1988) found that the scatter of peak acceleration data about the median attenuation relationship decreased with increasing magnitude. This effect has been reported in previous studies of crustal earthquakes (*e.g.*, Sadigh *et al.*, 1986; Abrahamson, 1988). Youngs *et al.* (1995) conducted a rigorous examination of California strong motion data using the random effects regression model and concluded that both inter-event and intra-event components of ground motion variability are magnitude dependent. The need for such magnitude dependence in the subduction zone data set was investigated by fitting linear relationships of the form $\tau = V_1 + V_2\mathbf{M}$ and $\sigma = V_3 + V_4\mathbf{M}$ to the variance terms of (1) and (2). We found that, using the likelihood ratio test (Seber and Wild, 1989), the null hypothesis that $V_2 = V_4 = 0$ can be rejected at the 1 percent significance level. We also found that the variance in the updated data set is larger than previously reported by Youngs *et al.* (1988). The resulting total variance for PGA was approximated by a linear function of **M** (Table 2).

The variance for SA was computed for the individual periods using the coefficients listed in Table 2 to define the median attenuation relationships. The resulting estimates were somewhat lower than the values obtained for PGA. Examination of the analysis results indicates that the inter-event components of the variance were nearly zero for most periods. This result is likely due to the limited number of earthquakes represented in the spectral ordinate data set.

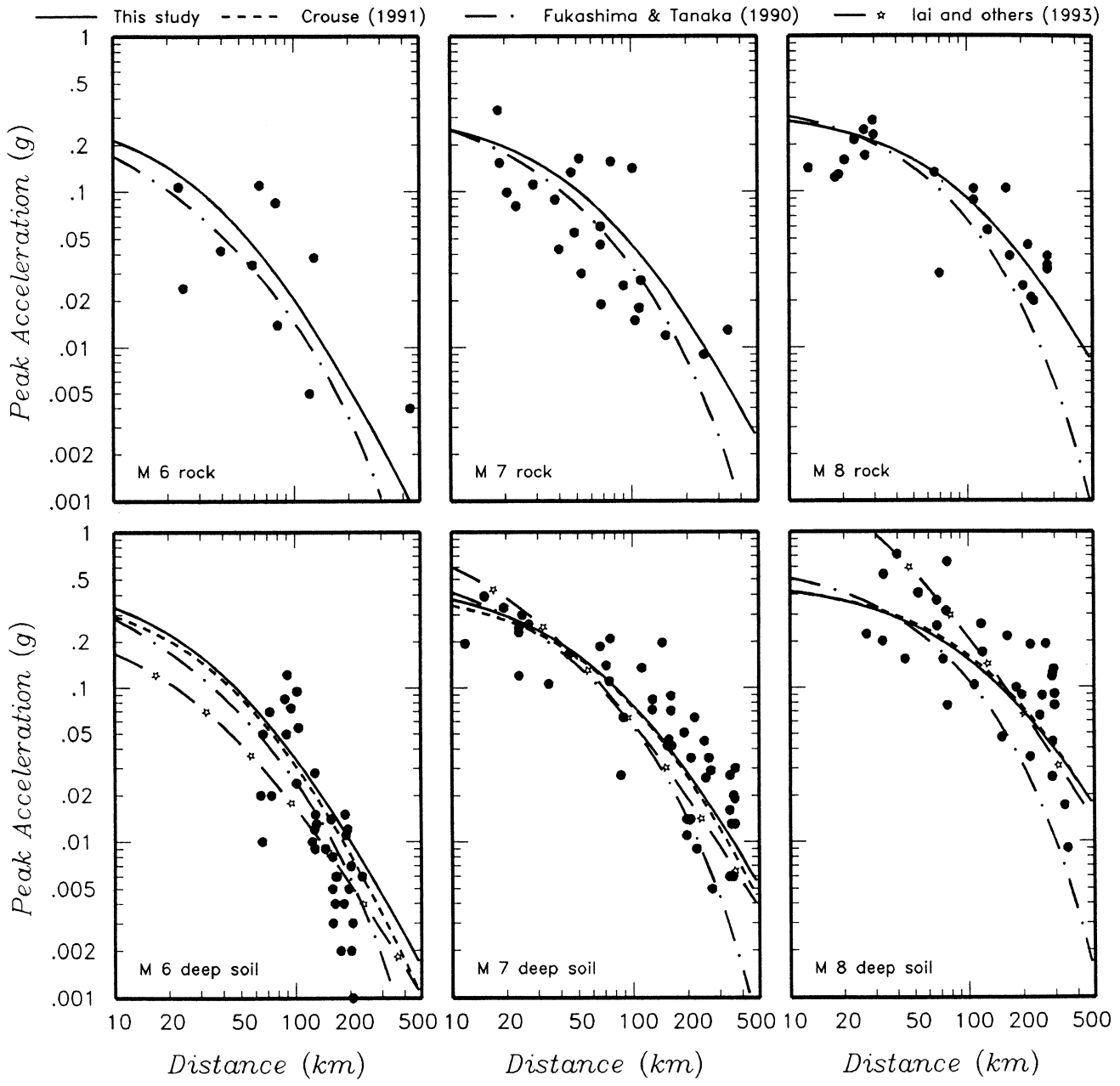

▲ **Figure 6.** Comparison of PGA attenuation relationships for rock and deep soil sites. Data are from Figure 2. The points are the PGA values from Figure 2 for the listed magnitude ±0.2 units.

Therefore, we increased the total variance for the spectral ordinates to account for an inter-event component of variance estimated from the peak acceleration data. The resulting relationships are listed in Table 2.

DISCUSSION

The attenuation relationships developed in this study are considered appropriate for earthquakes of magnitude **M** 5 and greater and for distances to the rupture surface of 10 to 500 km. The attenuation models indicate that for large events at large distances, one should expect that the peak motions from subduction zone earthquakes will be larger than those predicted using attenuation relationships for shallow crustal earthquakes. The difference between these types of earthquakes increases as the size of the earthquake increases. At small source-to-site distances, the empirical models developed in this study predict that the peak motions from interface earthquakes are lower than those for shallow crustal earthquakes. However, the near field data are very limited and numerical simulations indicate that peak motions may be similar to those predicted using shallow crustal earthquake attenuation relationships. Therefore, we suggest that one should consider estimates of peak motions

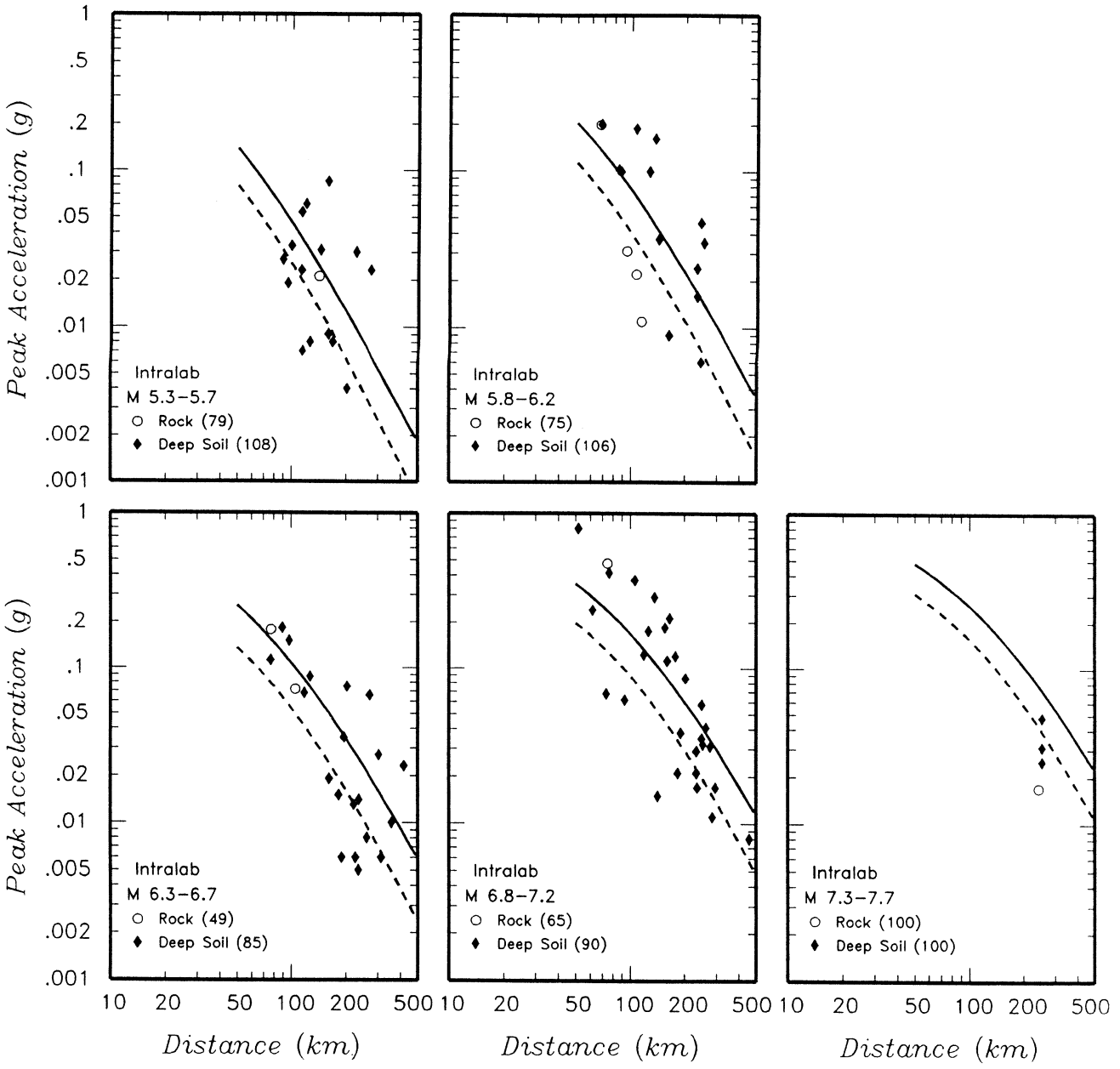

▲ **Figure 7.** Comparison of PGA values predicted using attenuation models listed in Table 2 and the empirical data for intraslab earthquakes. Numbers in parentheses give the average depth of earthquakes in each data subset. The solid line is the attenuation relationship fit to deep soil site data and the dashed line is the relationship fit to the rock data.

in the near field of interface earthquakes using both the models developed in this study and those obtained using attenuation relationships for shallow crustal earthquakes.

Because of the very limited number of processed intraslab recordings, the spectral shapes listed in Table 2 are based primarily on interface earthquake data. The attenuation coefficients presented by Crouse (1991) indicate that PGA values increase with earthquake depth but long period SA values decrease with increasing earthquake depth. If the larger PGA values for intraslab earthquakes are a result of higher stress drops for events rupturing oceanic crust, then one would expect that the difference between interface and intraslab motions would decrease with increasing spectral period. Thus, the attenuation relationships for SA for intraslab earthquakes listed in Table 2 may be somewhat conservative at longer periods.

REFERENCES

Abrahamson, N.A. (1988). Statistical properties of peak ground accelerations recorded by the SMART1 array, *Bull. Seism. Soc. Am.*, **78**, 26–41.

Abrahamson, N.A., and R.R. Youngs (1992). A stable algorithm for regression analysis using the random effects model, *Bull. Seism. Soc. Am.*, **82**, 505–510.

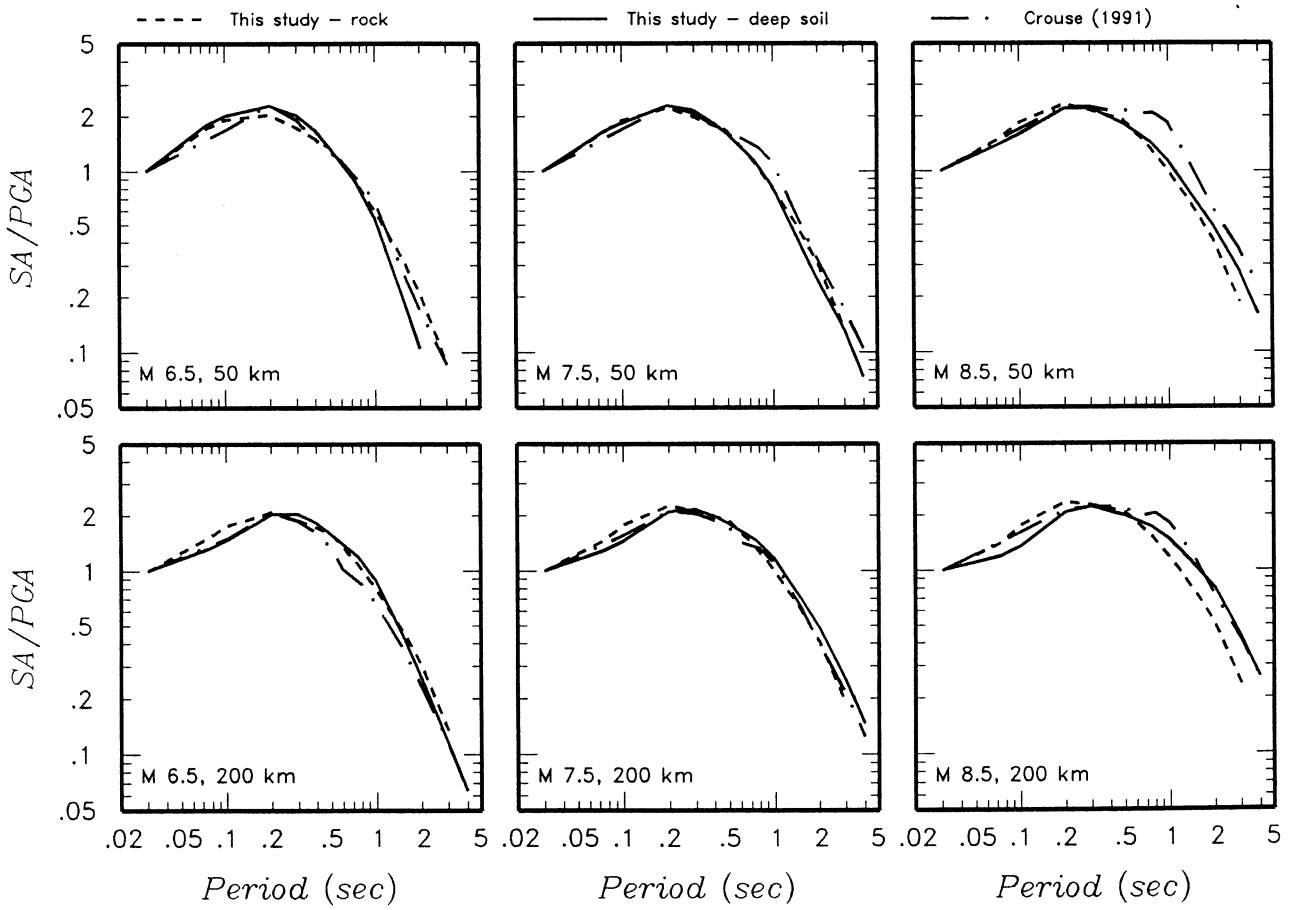

▲ **Figure 8.** Acceleration response spectral shapes (SA/PGA, 5% damping) for rock and deep soil sites computed using the relationships listed in Table 2. Also shown are spectral shapes computed using the attenuation relationships developed by Crouse (1991).

Boore, D.M., W.B. Joyner, and T.E. Fumal (1993). Estimation of response spectra and peak accelerations from western North American earthquakes, U.S. Geological Survey Open-File Report 93-509, 72 p.

Brillinger, D.R., and H.K. Preisler (1985). Further analysis of the Joyner-Boore attenuation data, *Bull. Seism. Soc. Am.*, **75**, 611–614.

Crouse, C.B. (1991). Ground-motion attenuation equations for earthquakes on the Cascadia subduction zone, *Earthquake Spectra*, **7**, 210–236.

Crouse, C.B., Y.K. Vyas, and B.A. Schell (1988). Ground motions from subduction-zone earthquakes, *Bull. Seism. Soc. Am.*, **78**, 1–25.

Fukushima, Y., and T. Tanaka (1990). A new attenuation relation for peak horizontal acceleration of strong earthquake ground motion in Japan, *Bull. Seism. Soc. Am.*, **80**, 757–783.

Hanks, T.C., and H. Kanamori (1979). A moment magnitude scale, *J. Geophys. Res.*, **84**, 2,348–2,350.

Humphrey, J.R., W.J. Silva, and R.R. Youngs (1993). Factors influencing site-specific ground motion estimates for the 1985 *M* 8.1 Michoacan earthquake (abs.), *Seism. Res. Lett.*, **64**, 17.

Iai, S., Y. Matsunga, T. Morita, H. Sakurai, E. Kurata, and K. Mukai (1993). Attenuation of peak ground acceleration in Japan, in *Proc. Int. Workshop on Strong Motion Data*, Menlo Park, California, December 13–17, 2, 3–21.

Iwasaki, T., T. Kataymas, K. Kawashima, and M. Saeki (1978). Statistical analysis of strong-motion acceleration records obtained in Japan, in *Proc. Second Int. Conf. on Microzonation for Safer Construction, Research, and Application, II*, 705–716.

Joyner, W.B., and D.M. Boore (1981). Peak horizontal acceleration and velocity from strong-motion records including records from the 1979 Imperial Valley, California earthquake, *Bull. Seism. Soc. Am.*, **71**, 2,011–2,038.

Joyner, W.B., and D.M. Boore (1993). Methods for regression analysis of strong-motion data, *Bull. Seism. Soc. Am.*, **83**, 469–487.

Krinitzky, E.L., F.K. Chang, and O.W. Nuttli, references in Krinitzky, E.L. (1987). Empirical relationships for earthquake ground motions in Mexico City, in *Proc. ASCE Conf.: The Mexico Earthquake—1985, Factors Involved and Lessons Learned*, Mexico City, September 19–20, 1986.

Molas, G.L., and F. Yamazaki (1995). Attenuation of earthquake ground motions in Japan including deep focus events, *Bull. Seism. Soc. Am.*, **85**, 1,343–1,358.

Sadigh, K., (1979). Ground motion characteristics for earthquakes originating in subduction zones and in the western United States, in *Proc. Sixth Pan Amer. Conf.*, Lima, Peru.

Sadigh, K., C.-Y. Chang, N.A. Abrahamson, S.J. Chiou, and M.S. Power (1993). Specification of long-period ground motions: updated attenuation relationships for rock site conditions and adjustment factors for near-fault effects, in *Proc. ATC-17-1 Seminar on Seismic Isolation, Passive Energy Dissipation, and Active Control*, March 11-12, San Francisco, California, 59–70.

Sadigh, K., J.A. Egan, and R.R. Youngs (1986). Specification of ground motion for seismic design of long period structures (abs.), *Earthquake Notes*, 57, n. 1, 13. Relationships printed in W.B. Joyner

and D.M. Boore (1988). Measurement, characterization, and prediction of strong ground motion, in *Earthquake Engineering and Soil Dynamics II—Recent Advances in Ground Motion Evaluation*, ASCE Geotechnical Special Publication 20, 43–102.

Seber, G.A.F., and C.J. Wild (1989). *Nonlinear Regression*, John Wiley and Sons, New York.

Silva, W.J. (1991). Global characteristics and site geometry, in *Proc. NSF/EPRI Workshop on Dynamic Soil Properties and Site Characterization*, Electric Power Research Institute Research Project NP-7337.

Silva, W.J., and C.L. Stark (1992). Source, path, and site ground motion model for the 1989 *M* 6.9 Loma Prieta earthquake, research report prepared for the California Division of Mines and Geology.

Tichelaar B.W., and L.J. Ruff (1993). Depth of seismic coupling along subduction zones, *J. Geophys. Res.*, **98**, 2,017–2,037.

Vyas, Y.K., C.B. Crouse, and B.A. Schell (1984). Ground motion attenuation equations for Benioff zone earthquakes offshore Alaska (abs.), *Earthquake Notes*, **55** (1), 17.

Wyss, M., and R.E. Habermann (1982). Conversion of m_b to M_S for estimating the recurrence time of large earthquakes, *Bull. Seism. Soc. Am.*, **72**, 1,651–1,662.

Youngs, R.R., N.A. Abrahamson, F. Makdisi, and K. Sadigh (1995). Magnitude dependent dispersion in peak ground acceleration, *Bull. Seism. Soc. Am.*, **85**, 1,161–1,176.

Youngs, R.R., S.-J. Chiou, W.L. Silva, and J.R. Humphrey (1993). Strong ground motion attenuation relationships for subduction zone earthquakes based on empirical data and numerical modeling (abs.), *Seism. Res. Lett.*, **64**, 18.

Youngs, R.R., S.M. Day, and J.P. Stevens (1988). Near field motions on rock for large subduction zone earthquakes, in *Earthquake Engineering and Soil Dynamics II—Recent Advances in Ground Motion Evaluation*, ASCE Geotechnical Special Publication 20, 445-462.

Geomatrix Consultants
100 Pine St., 10th Floor
San Francisco, CA 94111
(R.R.Y., S.-J.C.)

Pacific Engineering and Analysis
311 Pomona St.
El Cerrito, CA 94530
(W.J.S.)

Lahontan GeoScience Inc.
21380 Castle Peak Rd.
Reno, NV 89511-7119
(J.R.H.)